Available online at www.sciencedirect.com
SCIENCE DIRECT®
ELSEVIER
International Journal of Multiphase Flow 31 (2005) 869–896
International Journal of Multiphase Flow
www.elsevier.com/locate/ijmulflow

Co-current stratified gas–liquid downflow—Influence of the liquid flow field on interfacial structure

J.S. Lioumbas, S.V. Paras *, A.J. Karabelas

Department of Chemical Engineering, Aristotle University of Thessaloniki, Univ. Box 455, GR 54124 Thessaloniki, Greece

Received 1 February 2005; received in revised form 11 May 2005

Abstract

The transition from smooth to wavy stratified flow is studied for various pipe inclination angles with the aim to contribute to the realistic modeling and simulation of long distance two-phase pipe flow. The influence of the liquid flow field on interfacial structure is studied through local axial velocity measurements in the liquid phase in conjunction with other liquid layer characterization experiments. Observations based on fast-video recordings, are used to identify the main patterns of wave evolution. Liquid layer thickness time records are acquired using a parallel wire conductance technique from which mean layer thickness, *RMS* and power spectra of the fluctuations, as well as wave celerities are calculated. Laser Doppler Anemometry (*LDA*) is employed to investigate the flow structure in the thin liquid layer both with and without interfacial shear induced by a co-current gas flow. The results reveal the influence of the liquid flow field development on the interfacial structure. In particular, the new data of axial velocity profiles and liquid layer characteristics suggest that the onset of the interfacial waves is strongly affected by the liquid flow structure, possibly by the laminar to turbulent transition within the layer.

Keywords: Stratified flow; Turbulent transition; Free flowing layer; Inclined pipe

* Corresponding author. Tel.: +30 2310 996174; fax: +30 2310 996209.
E-mail address: paras@cheng.auth.gr (S.V. Paras).

0301-9322/$ - see front matter © 2005 Elsevier Ltd. All rights reserved.
doi:10.1016/j.ijmultiphaseflow.2005.05.002

1. Introduction

The co-current stratified gas–liquid downflow is a flow regime frequently encountered in long distance hydrocarbon pipelines, as well as in transfer lines in process plants. The accurate characterization of both the structure of the gas–liquid interface and of the flow field inside the liquid layer are considered essential to understand the mechanisms involved in the evolution of waves at the transition from smooth to wavy stratified flow regime.

Extensive research work, both experimental and theoretical, carried out over the last three decades suggests that the rate of momentum, heat and mass transfer is strongly influenced by the liquid layer characteristics and especially by the waviness of the gas–liquid interface. Barnea et al. (1980) and Brauner and Maron (1992) studied the flow patterns for gas–liquid flow in inclined pipes and, by comparing their results with the Taitel and Dukler (1976) theoretical model, concluded that the latter is not capable of predicting the transition from smooth to wavy stratified flow as it does not take into account the waves generated by gravity in downward flow. Moreover, Barnea et al. (1980), who conducted experiments in two-phase flow in inclined and horizontal pipes, reported that the appearance of interfacial waves depends on the liquid layer thickness and that the wave amplitude is significantly affected by the pipe inclination. Andreussi and Persen (1987) proposed semi-empirical correlations for the interfacial friction factor and the liquid holdup in gas–liquid co-current flow in slightly downward inclined 5 cm i.d. pipe. The stability analysis performed by Giovine et al. (1991) for a liquid flowing down an inclined circular tube suggests that the liquid layer is smooth and undisturbed up to an h/D value 0.50 for laminar and 0.85 for turbulent flow. Ng et al. (2001) pointed out the lack of work on free surface pipe flow and used *CFD* to evaluate the integral and local gravity-driven laminar flow in a partially filled pipe.

To enhance our physical understanding of the more complicated case of co-current gas–liquid flow in inclined pipes, it is considered advantageous to utilize relevant information on wavy free flowing layers. Despite progress made in recent years, significant gaps still exist in understanding and modeling the evolution of such free flowing layers. The latter were first studied by Kapitza (father and son), who conducted simple experiments on an inclined plane at a Reynolds number of about 100 (Fulford, 1964). This early work was followed by a plethora of studies regarding liquid layer flow on inclined or vertical planes (e.g. Binnie, 1957; Jones and Whitaker, 1966; Telles and Dukler, 1970; Vlachogiannis and Bontozoglou, 2002). However, for inclined pipes, systematically obtained data on free flowing layer thickness for various diameters and inclination angles in a range of low to moderate Reynolds numbers are limited in the literature. Wilkes and Nedderman (1962), working with glycerin solutions in a 3 m vertical tube (25 mm i.d.), made measurements of the velocity profiles within thin wavy layers and concluded that the profile remains parabolic, i.e. similar to a Nusselt flat layer. Stainthorp and Allen (1965) performed a set of experiments for very low Reynolds numbers (4–45) using water inside a 76 cm long vertical glass tube (i.d. = 3.45 cm) and reported that, for naturally excited waves, the wave profile, wavelength and wave celerity change significantly downstream of the wave inception line. Giovine et al. (1991) investigated theoretically the stability of liquid flow down an inclined pipe using linear stability analysis and concluded that after a certain value of liquid height the flow becomes unstable. The work of Karimi and Kawaji (1998, 1999) provided detailed data sets of the liquid flow field structure in a vertical tube. These authors concluded that the large waves on the gas–liquid interface and the flow field inside the liquid layer are strongly interrelated. Recently Mouza et al.

(2003) studied experimentally the influence of small tube diameter on a free flowing layer in inclined tubes and proposed an analytical expression for estimating the liquid layer thickness. Lioumbas et al. (2004) obtained complete sets of detailed data on water layer gravity-driven flow inside slightly inclined pipes of various diameters, for various liquid flow rates.

The flow field structure of the liquid layer has been extensively studied in *horizontal* pipe stratified two-phase flows (e.g. Paras and Karabelas, 1991; Banat, 1992; Lorencez et al., 1997; Wongwises and Kalinitchenko, 2002). However, studies concerning the flow structure under the wavy gas–liquid interface (i.e. inside thin liquid layers) in *inclined* pipes are not available in the literature, probably due to the difficulty in obtaining accurate velocity measurements inside such very thin layers.

The scope of this work is to study the transition from smooth to wavy stratified flow for various pipe inclination angles and gas–liquid flow rates. The study of the liquid flow field structure, through local axial velocity measurements, in conjunction with the liquid layer characterization experiments is aimed at elucidating the influence of the liquid flow field on the interfacial structure. Experiments are also conducted in the *absence* of gas, i.e. before introducing the complication of co-current gas–liquid flow. Thus, experimental data on free flowing and on co-currently flowing gas–liquid layers are reported, various statistical quantities are extracted from layer thickness time records and local liquid axial velocity measurements (e.g. layer height, axial velocity profiles, statistical characteristics) that facilitate characterization of liquid layer behavior.

2. Experimental setup and procedures

Experiments are conducted at ambient temperature and pressure in a flow rig comprised of 24 mm i.d. Plexiglas® tube with a 7 m long straight section, which can be inclined up to 15° with respect to the horizontal. A schematic layout of the flow loop is shown in Fig. 1. The gas and liquid flow rates are measured using a bank of calibrated rotameters with accuracy better than ±1%. Properly conditioned air (i.e. filtered and dried) is supplied to the rig, while filtered tap water is recirculated by a centrifugal pump. Both phases are introduced through a carefully designed entrance section in order to minimize disturbances and promote development of stratified flow. The superficial velocities are varied in the range $U_{SL} = 0.2$–5 cm/s for the liquid and $U_{SG} = 0$–20 m/s for the gas, covering the stratified flow regime as well as the transition from smooth to wavy flow.

Liquid layer thickness is measured using the parallel wire conductance probe method, which is based on the inverse proportionality between electrical resistance of the liquid layer and its thickness. The specially designed test section, which is constructed to accommodate parallel wire conductance probes, is positioned approximately 6 m away from the mixing section of the two phases, where the flow can be considered developed. The conductance probe consists of two long parallel chromel wires (0.3 mm in diameter and 2 mm apart) placed on a plane vertical to the pipe axis, extending along the entire pipe diameter. In order to obtain wave celerity measurements, two probes are employed placed 3 cm apart. The probes are connected to an electronic circuit, comprised of a custom-made analyzer and a 25 kHz function generator. The liquid conductivity is measured both prior to and after each set of experiments and a correction factor is incorporated into the layer thickness calculations to compensate for temperature effects. The accuracy of the

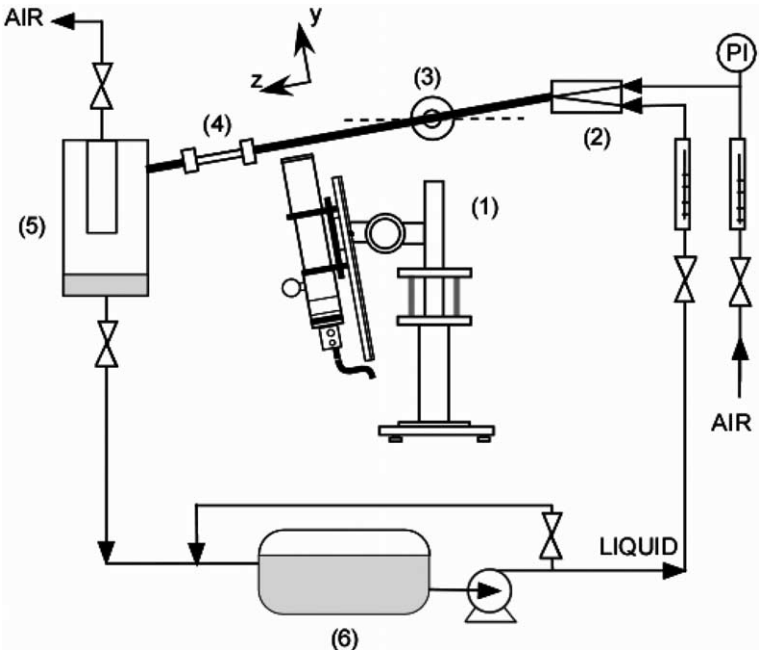

Fig. 1. Experimental flow loop: (1) *LDA* setup; (2) gas–liquid entrance test section; (3) rotating support; (4) conductance probe test section; (5) phase separator; (6) liquid storage tank.

measurements is estimated to be around ±10% taking into account uncertainties in the calibration procedure. The statistical quantities and other parameters of the layer thickness time records are calculated from 10,000-point samples, obtained over a period of 100 s with a 100 Hz sampling frequency. Paras and Karabelas (1991) give a detailed description of the conductance probe method.

An *LDA* setup, which operates in the fringe mode, is employed to make measurements of local axial velocities within the liquid phase. The non-intrusive *LDA* technique is suitable for detailed local velocity measurements in very thin films since it permits measurements very close to the wall (~100 μm) with very good spatial resolution (~70 μm). A 5 W Argon-Ion laser source is used, having a wavelength of 514.5 nm and a maximum power of 2 W. The green beam from this source is split into two identical beams by an optical arrangement supplied by DANTEC. A special support unit for the *LDA* system, constructed in this laboratory, allows precise spatial movement of the measuring volume (Fig. 1). A more detailed arrangement of the *LDA* system and the signal analysis method applied in this study is given elsewhere (Paras and Karabelas, 1992).

In an effort to gain insight into the basic mechanisms contributing to wave evolution, direct visual observations were made over a fairly broad range of flow rates, as well as recordings using a Redlake MotionScope PCI® high-speed camera to capture details of the flow. Pictures were taken at a speed of 250 frames/s and a shutter rate of 1/1000.

Throughout this study two different definitions of the Reynolds number are used, i.e. the *superficial* $Re_{SL} = U_{SL}D/\nu_L$ and the *actual* $Re_L = U_L D_L/\nu_L$ based on the superficial liquid velocity, U_{SL}, and on the mean liquid velocity, U_L, respectively. D is the pipe diameter, while D_L and ν_L are the hydraulic diameter and the kinematic viscosity of the liquid phase, respectively.

3. Free flowing layer in inclined pipes

3.1. Visual observations

In this section an overview of the flowing liquid layer interfacial structure is presented, obtained by visual observations. Four distinct flow regions can be readily identified:

- For the smallest Reynolds numbers employed, small-amplitude waves are observed on the liquid surface (*Region I*). Patnaik and Blanco (1996) have also described this kind of waves in detail even though their study refers to flowing layers on inclined plates.
- As the liquid flow rate increases, the liquid interface turns practically smooth and undisturbed (*Region II*). Park and Nosoko (2003) reported a similar behavior, i.e. transition from a wavy to an undisturbed interface with increasing flow rate, even though they deal with free falling layer characteristics inside *vertical* pipes for $Re_L \sim 400$.
- At still higher Re_L two-dimensional, large-amplitude, relatively long-wavelength waves (henceforth referred to as *solitary waves*) separated by an undisturbed liquid layer make their appearance at a distance of approx. 30–50 pipe diameters from the liquid entrance, traveling along the pipe on the liquid interface (*Region III*). These waves retain their original shape while traveling along the pipe. A *critical* Reynolds number, Re_{LC}, obtained by visual observations, is associated with the first appearance of solitary waves.
- As the flow rate increases further, the large waves become more frequent, retain their original amplitude and tend to merge forming 3D structures (*Region IV*).

The above behavior is observed for all inclination angles tested, as well as for various pipe diameters (24, 32 and 60 mm) (Lioumbas et al., 2004).

3.2. Liquid layer characteristics

Using the experimental procedures described in Section 2, the free flowing liquid layer thickness was measured for an inclination range, β, of 1–9° for the 24 mm i.d. and for liquid flow rates, Q_L, from 3.3×10^{-6} to 42×10^{-6} m^3/s. In Fig. 2 typical liquid layer traces for the 24 mm pipe at $\beta = 1°$ and 5° are presented, where the regions described in the previous section are readily observed. Indeed, for $Re_L = 1000$ (Fig. 2a) the trace corresponds to *Region I*, where small-amplitude gravitational waves appear on the liquid surface. As the liquid flow rate increases (Fig. 2b) the liquid interface turns practically smooth and undisturbed (*Region II*, $Re_L = 1700$). When $Re_L = 2200$ is reached (Fig. 2c) solitary waves (as defined in Section 3.1) are the dominant feature (*Region III*). A further flow rate increase ($Re_L = 4000$) results in a flow pattern corresponding to *Region IV* (Fig. 2d), where high-frequency small-amplitude 3D waves can be easily observed. It should be pointed out that the aforementioned four Regions (based on the layer thickness traces) are observed for all inclination angles tested.

The time series of the thickness data are statistically analyzed to obtain the main layer characteristics, namely the mean (h_{mean}) and the root mean square (h_{rms}) of the thickness. The celerity (c) of the waves is calculated by cross-correlating two signals, recorded simultaneously at two neighboring locations (i.e. 30 mm apart). The modal frequency of the waves (f_m) is calculated from the

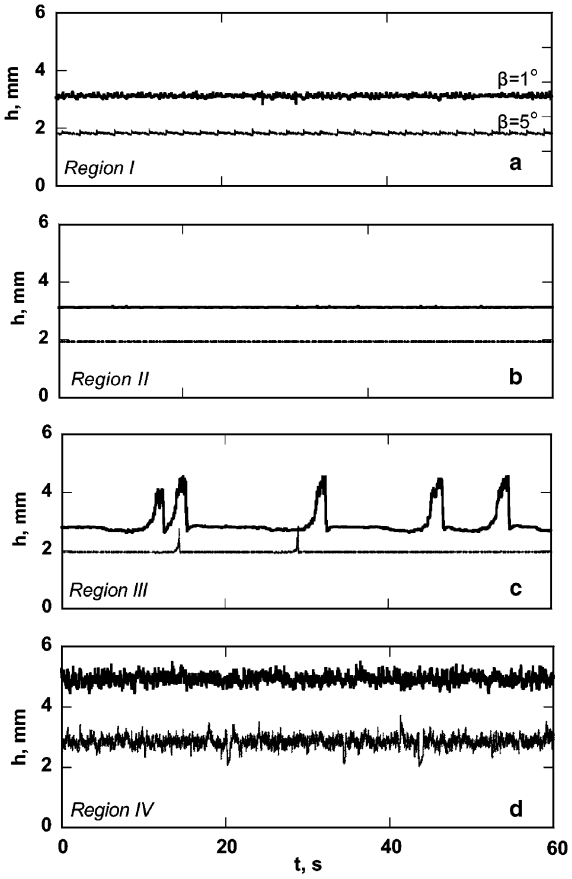

Fig. 2. Typical layer thickness traces for $\beta = 1°$ and 5°: (a) $Re_L = 1000$; (b) $Re_L = 1700$; (c) $Re_L = 2200$; (d) $Re_L = 4000$.

power spectral density (*PSD*) of the layer thickness time series. The PSD is obtained by averaging modified periodograms (Paras and Karabelas, 1991). The uncertainty of the computed spectra is estimated to be ±12% and their resolution is approximately 0.2 Hz. Typical results of the quantities described above are listed in Table 1.

In Fig. 3 the calculated h_{mean} results are presented as a function of Re_L for three typical inclination angles. It is evident that h_{mean} increases with Re_L and decreases as the inclination angle increases. The procedure followed by Mouza et al. (2003), which is valid for a laminar free flowing layer in a pipe, is employed to compute the mean layer thickness, using Q_L, D, β, and fluid physical properties as input quantities. As shown in Fig. 3, there is a fairly good agreement between measured values and the predictions from this theoretical model *only* for a Reynolds number region $Re_L < 2200$. Obviously, for the larger liquid flow rates, where *Regions I* and *II* tend to disappear, this laminar model does not agree with the experimental data. To take into consideration both laminar and turbulent flow regimes, a modified force balance is employed (Appendix A). A comparison of the mean liquid layer thickness obtained from Eqs. (A.9) and (A.10) with experimental data is also presented in Fig. 3. As expected, for $Re_L < 2200$ both models give practically the same results, while for $Re_L > 2200$ the experimental data are in very good agreement with the

Table 1
Summary of results (free flowing layer)

1°					4°					8°				
Re_L	h_{mean} (mm)	h_{rms} (mm)	c (m/s)	f_m (Hz)	Re_L	h_{mean} (mm)	h_{rms} (mm)	c (m/s)	f_m (Hz)	Re_L	h_{mean} (mm)	h_{rms} (mm)	c (m/s)	f_m (Hz)
900	2.45	0.05	0.38	0.6	1120	1.65	0.03	0.42	0.7	1240	1.40	0.02	0.50	0.9
1300	2.72	0.00	0.00	0.0	1580	1.82	0.00	0.00	0.0	1750	1.56	0.00	0.00	0.0
1640	2.89	0.00	0.00	0.0	2020	2.05	0.00	0.00	0.0	2140	1.80	0.00	0.00	0.0
2080	3.00	0.00	0.00	0.0	2310	2.11	0.02	0.38	0.3	2540	1.94	0.02	0.41	0.2
2300	3.20	0.00	0.00	0.0	2650	2.23	0.04	0.33	0.1	2920	2.02	0.02	0.42	0.3
2510	3.34	0.03	0.35	0.2	2800	2.41	0.10	0.34	0.2	3280	2.03	0.09	0.43	0.4
2700	3.48	0.11	0.27	0.2	3300	2.69	0.26	0.34	0.2	3620	2.18	0.21	0.45	0.4
3000	3.85	0.34	0.28	0.2	3600	2.95	0.35	0.42	0.2	3960	2.34	0.23	0.67	0.4
3230	4.39	0.65	0.34	0.3	3900	3.08	0.27	0.55	0.3	4290	2.50	0.19	0.75	1.2
3700	4.95	0.24	0.50	0.4	4470	3.32	0.12	0.60	0.5	4920	2.73	0.09	0.75	1.7
4100	5.28	0.14	0.58	0.6	5000	3.54	0.12	0.64	0.8	5520	2.89	0.13	0.77	1.6
4520	5.50	0.14	0.58	0.7	5530	3.74	0.11	0.67	0.9	6100	3.08	0.13	0.81	1.9
5000	5.78	0.15	0.56	0.8	6040	3.95	0.11	0.75	1.0	6660	3.23	0.13	1.00	2.0
5300	6.06	0.15	0.60	0.9	6530	4.15	0.12	0.75	1.3	7200	3.38	0.12	1.00	2.1
6200	6.63	0.16	0.60	1.2	7700	4.66	0.13	0.83	2.0	8510	3.76	0.12	1.03	2.3

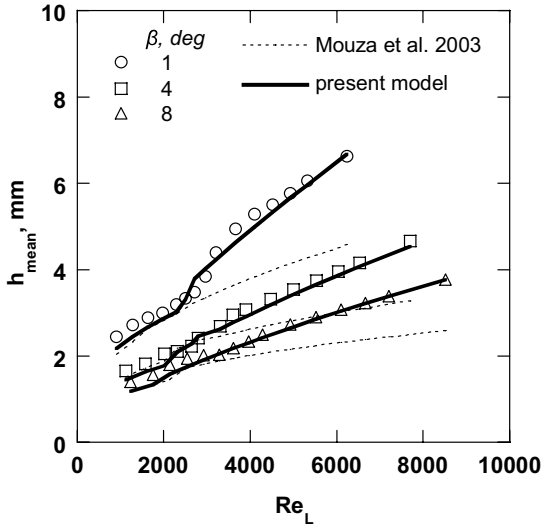

Fig. 3. h_{mean} vs. Re_L, comparison with model predictions for various β.

proposed model. Consequently, the new model, which takes into account the turbulent behavior of the liquid layer, is considered more appropriate for the study of free flowing liquid layers in pipes for moderate Re_L ($Re_L > 1000$). The fact that the data of the present study (for all angles tested) are in good agreement with the model predictions could be considered as a piece of evidence (to be subsequently complemented) that the appearance of solitary waves might be related with the *transition* from laminar to turbulent flow.

In Fig. 4 the dependence of h_{rms} on Re_L is presented for various inclination angles. The regions, identified earlier both by visual observations and liquid height measurements, can also be distinguished as follows:

- *Region I*. In this region, where the small-amplitude gravitational waves are observed, h_{rms} values are relatively low. The wave celerity and the wave frequency of these waves have values in the range of ~0.4 m/s and ~0.4 Hz, respectively, for $\beta = 1°$, but they tend to increase with β (Table 1).
- *Region II*. With increasing flow rate, the h_{rms} values become even smaller than those observed in *Region I*, since the small-amplitude waves tend to diminish and the liquid interface becomes practically smooth.
- *Region III*. This region corresponds to a sharp increase of the h_{rms} values, a behavior attributed to the presence of solitary waves (Fig. 2c) which are traveling down the pipe with celerity $c \sim 0.35$ m/s and modal frequency $f_m \sim 0.2$ Hz (Table 1). As β increases, c and f_m also increase (Table 1). As shown in Fig. 4 for higher liquid flow rates, a maximum value of h_{rms} is reached, which decreases as the pipe inclination increases (Table 1). A further Re_L increase leads to a strong reduction of the h_{rms} values, a fact attributed to the presence of more frequent solitary waves, which tend to merge resulting in higher h_{mean} (Fig. 3) and reduced h_{rms} values (Fig. 4).
- *Region IV*. At still higher liquid flow rates, the h_{rms} values become practically independent of Re_L since the liquid interface is dominated by small-amplitude high frequency ($f_m \sim 1.2$ Hz) 3D waves which travel down the pipe with $c \sim 0.6$ m/s (for $\beta = 1°$). 3D waves are traveling faster along the pipe and their modal frequency increases with β (Table 1).

It is interesting that the critical Reynolds number (Re_{LC}), which is related to the first appearance of solitary waves, is in the narrow range of 2100–2300 (Table 2), which in single phase pipe flow is associated with the transition from laminar to turbulent flow (e.g. Wygnaski and Cham-

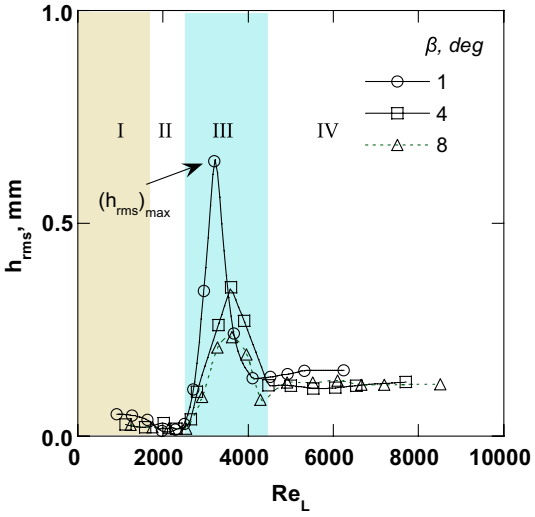

Fig. 4. Effect of pipe inclination on h_{rms} values.

Table 2
Effect of pipe inclination on Re_{LC}, for various pipe diameters (free flowing layer)

D (mm)	β (deg)								
	1	2	3	4	5	6	7	8	9
24	2200	2300	2200	2200	2150	2200	2100	2300	2250
32	2100	2200	2300						
60	2150	2200	2150						

pagne, 1973). Consequently, with the intention of elucidating the relation between the flow structure inside the liquid layer and the onset of the solitary waves, the flow field under the interface is studied in order to determine the type of flow prevailing for the various liquid flow rates tested.

3.3. Axial velocity measurements in free flowing layers

The axial velocity (U) profile is measured in the liquid layer, at a pipe cross section along its vertical axis of symmetry, for a range of β from 1° to 4° with the aforementioned *LDA* setup. In these measurements the mean data acquisition rate varied in the range 100–200 Hz, depending on the local mean velocity and the distance from the pipe wall, while the sample size for each run was 6000 data points. The data acquisition, the statistical analysis and the signal reconstruction methods for unequally spaced Doppler signals are presented in detail elsewhere (Paras and Karabelas, 1992).

It must be noted that the *LDA* measuring station is placed 20 cm *upstream* of the layer thickness measuring test section made of translucent material that does not allow *LDA* measurements. However, taking into account the calculated wave celerity, the time-lag between the *LDA* and the liquid layer measurements can be specified. Consequently, practically *simultaneous* measurements of the liquid layer thickness and the axial velocity can be obtained. In Fig. 5 typical axial velocity traces at various normalized distances (y/h_{mean}) from pipe wall are presented, for various liquid flow rates corresponding to *Regions I, II, III* and *IV*. It is noted that only the U measurements made at the location *closest* to the liquid interface (highest y/h_{mean}) can be considered simultaneous with the liquid layer trace.

In Fig. 5a, axial velocity measurements are presented for a liquid flow rate corresponding to *Region I*, where the liquid interface is dominated by small-amplitude gravitational waves. It is evident that the local streamwise velocity trace exhibits significant resemblance to the liquid layer fluctuations, as Karimi and Kawaji (1999) have also pointed out for the case of free falling laminar films in vertical pipes. It is obvious that a liquid layer wave crest corresponds to an axial velocity wave trough (marked with arrows) and that the streamwise velocity increases with distance from the wall. As the liquid flow rate increases further (*Region II*) both the liquid interface and the axial velocity become flat and undisturbed (Fig. 5b).

At higher flow rates (*Region III*, $Re_L = 2200$), the first solitary waves appear on the liquid interface and the local axial velocity under each solitary wave is significantly reduced (Fig. 5c). After the passing of a solitary wave, the interface becomes smooth and undisturbed and the liquid axial velocity increases, as expected, to satisfy mass balance. Similar observations of free falling films by Karimi and Kawaji (1999) reveal that at the laminar-to-turbulent transition two distinct regions

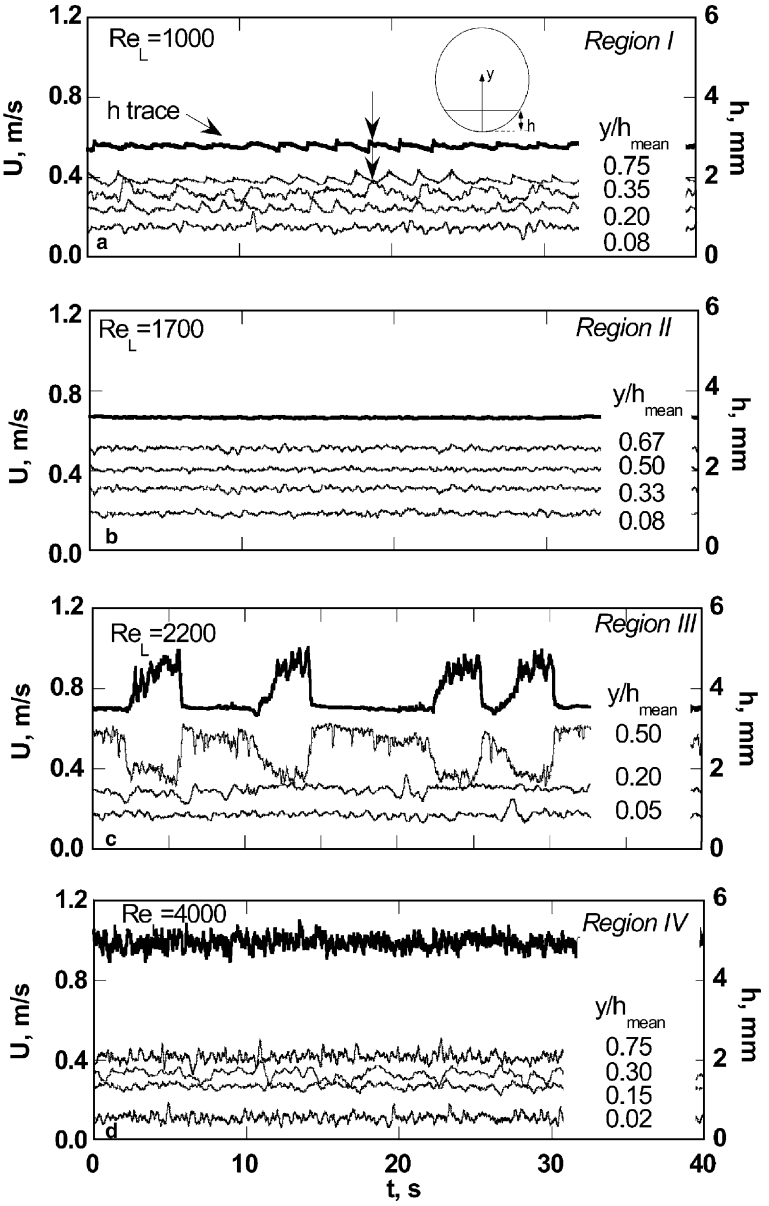

Fig. 5. Axial velocity measurements at various distances (y/h_{mean}) from pipe wall for various liquid flow conditions (thick line corresponds to thickness trace; $\beta = 1°$).

can be readily discerned: i.e. the *smooth* film region, where insignificant changes in the streamwise velocity are observed under the undisturbed interface, and the *wavy* region, where significant changes in the streamwise velocity are identified. Furthermore, it is evident (Fig. 5c) that the axial velocity disturbances are more pronounced near the interface (i.e. at $y/h_{\text{mean}} = 0.50$) than near the pipe wall (i.e. at $y/h_{\text{mean}} = 0.05$). At still higher flow rates, the solitary waves tend to be more fre-

quent, evolving into 3D waves. The axial velocity traces (at various distances from pipe wall) are similar to the thickness trace as shown in Fig. 5d. The layer is thicker than that in the preceding region, whereas the local axial velocities, as expected, attain smaller values.

It is well known that the transition from laminar to turbulent flow occurs in an intermittent fashion, i.e. the flow is occasionally laminar or turbulent (e.g. Wygnaski and Champagne, 1973; Nino and Serio, 2000; Fowler and Howell, 2003). The physical character of this flow may be described by an *intermittency factor* (γ), which represents the fraction of time at which there is turbulent flow. Therefore $\gamma = 1$ means continuous turbulent flow and $\gamma = 0$ continuous laminar flow (Schlichting and Gersten, 1999). Similarly, an intermittency factor for a wavy liquid layer (γ_w) is defined as the fraction of total sampling time corresponding to the passage of large waves (Paras and Karabelas, 1991). Time records of axial velocity (at a distance $y = 2.0$ mm from pipe wall) and the corresponding liquid layer thickness measurements were statistically analyzed in order to calculate these intermittency factors. Fig. 6 shows that the intermittency of both the layer thickness and U, with respect to Re_L, follows the same sigmoid distribution. As expected, their value is zero in *Regions I* and *II*, since no waves exist on the liquid interface, but, with the appearance of large waves (*Region III*) both intermittency factors sharply increase to high values and, by further increasing Re_L, they approach unity (*Region IV*). It is noted that this behavior of the velocity intermittency factor is similar to that identified in the laminar-to-turbulent transition in single phase flow (Schlichting and Gersten, 1999).

Fig. 7a presents a typical plot of the axial velocity fluctuations, $U - \overline{U}$ vs. time (where $\overline{U}$ is the time-averaged axial velocity) for a transition Reynolds number ($Re_L = 2200$) at $y/h_{mean} = 0.5$; it is clear that the velocity fluctuations under each solitary wave are much greater than the smooth part of the film trace before and after a solitary wave. In Fig. 7b, h_{rms} and the root mean square (*RMS*) of velocity fluctuations (u') (at $y = 2.0$ and 0.3 mm) are plotted as a function of Re_L. It is interesting to notice that h_{rms} and u' display similar qualitative behavior when plotted vs. Re_L;

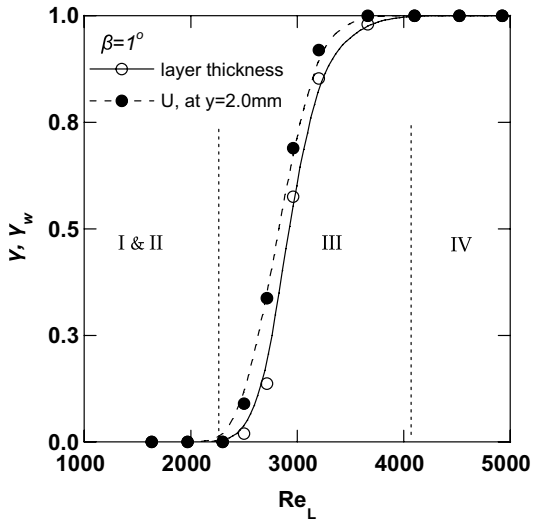

Fig. 6. Effect of Re_L on intermittency factors, γ, γ_w ($\beta = 1°$).

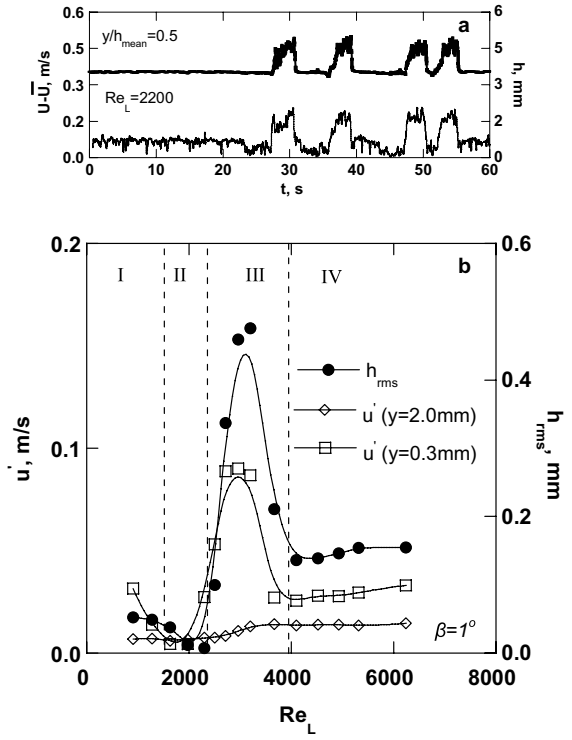

Fig. 7. (a) Effect of solitary wave passage on time dependent axial velocity fluctuations ($U - \overline{U}$); (b) Effect of Re_L, on h_{rms} and u'; $\beta = 1°$.

consequently, the four regions described in Sections 3.1 and 3.2 can be also identified. The relatively high values of u' and h_{rms} observed in *Region I* are attributed to the presence of the interfacial gravitational waves. As the liquid flow rate further increases, the interface becomes undisturbed (*Region II*) and both u' and h_{rms} values approach zero. The peak of both h_{rms} and u' observed in *Region III* corresponds to the same Re_L, and it is associated with the appearance of solitary waves. At higher Re_L (*Region IV*), both h_{rms} and u' values tend to be practically independent of the liquid flow rate. It is obvious that u' is more pronounced near the liquid interface than it is near the pipe wall, as was also shown in Fig. 5. From the above observations it is evident that there is a strong relation between the liquid flow field and the interfacial waves.

In order to further examine the flow structure under the interface *before* and *after* the passage of a solitary wave and to test the notion that its appearance is related to the laminar-to-turbulent transition, measurements of the axial velocity distribution (along the vertical diameter) are employed for various liquid flow rates. It is noted that the first local axial velocity measurement is conducted at $y = 100$ μm from the pipe wall. In Fig. 8 typical profiles $\overline{U}$ vs. the distance from the pipe wall (y) are presented for two inclination angles ($\beta = 1°$ and 4°). The measurements are compared with a solution of the simplified Navier–Stokes equations for partly filled laminar pipe flow, presented by Mouza et al. (2003). Although the experimental results for *Region II* are in good agreement with the analytical solution, those corresponding to *Region III* ($Re_L = 2300$) devi-

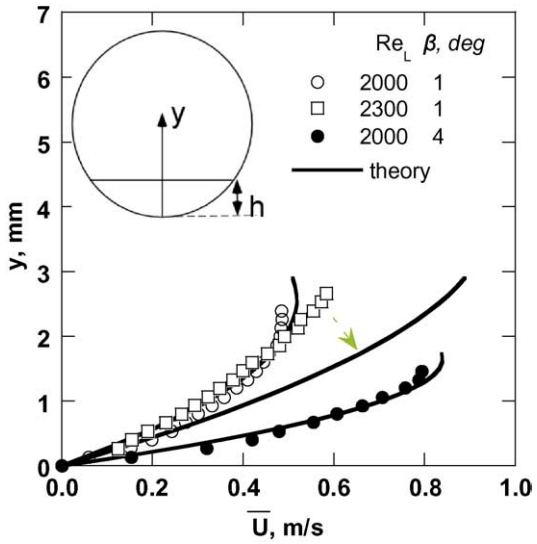

Fig. 8. Comparison of time-averaged axial velocity measurements with theoretical predictions; $\beta = 1°$ and 4°.

ate considerably. This is expected, since the theoretical solution does not take into account the solitary waves developing in *Region III*.

The velocity data are normalized with respect to the friction velocity (U^*) calculated by the procedure proposed by Paras and Karabelas (1992); i.e. it is assumed that there is a laminar sublayer for $y < 100$ μm so that

$$U^+ = y^+ \tag{1}$$

and

$$U^* = \sqrt{\frac{\nu U_{(y=100\,\mu m)}}{y}} \tag{2}$$

Using Eqs. (1) and (2) values of U^* are calculated from velocity data obtained very close to the wall (at $y = 100$ μm).

A typical distribution of the normalized velocities obtained for various liquid flow rates (for $\beta = 1°$) is presented in Fig. 9. The comparison with the von Karman universal velocity distribution for single-phase flow (Schlichting and Gersten, 1999) reveals that the flow is laminar for $Re_L = 2000$, turbulent for $Re_L = 5500$, while for $Re_L = 2300$ it appears to be in the transitional region. Additional evidence, that the flow is turbulent within the thin liquid layer for liquid flow rates corresponding to *Region IV* ($Re_L = 5500$), is the slope of the Power Spectral Density distribution (*PSD*) in logarithmic coordinates. It is shown (Fig. 10) that this slope equals $-5/3$ in the high frequency range as in the case of turbulent single phase flow; however, this is not observed for $Re_L = 2300$.

Fig. 11 presents the distribution of turbulence intensity (u'/U^*) as a function of the dimensionless distance from the pipe wall (y^+) for two typical Re_L. Both distributions exhibit a maximum value ~2 at $y^+ \sim 15$. This behavior is similar to the one reported for turbulent pipe flow, where

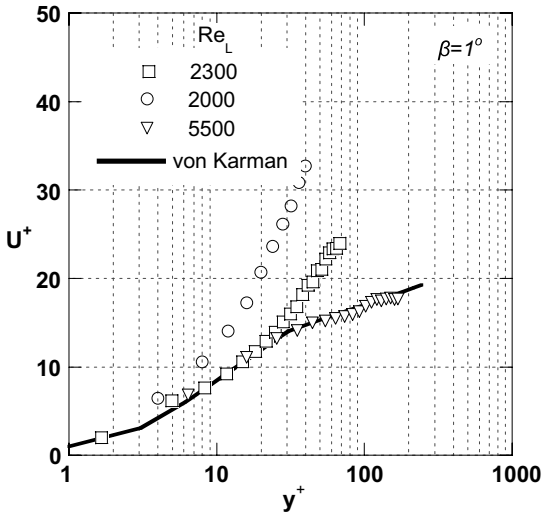

Fig. 9. Comparison of U^+ with von Karman universal velocity distribution for various Re_L; $\beta = 1°$.

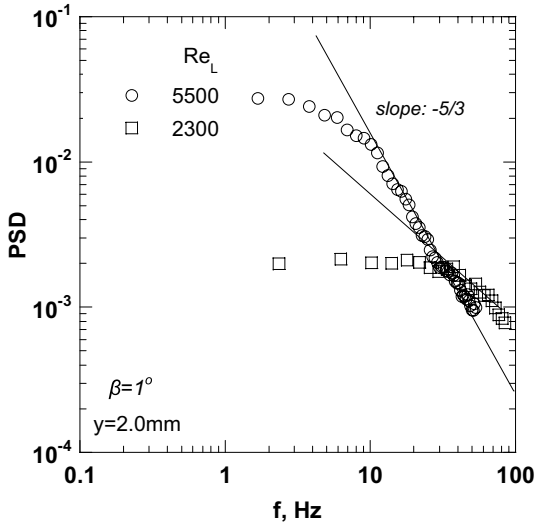

Fig. 10. Typical spectra of liquid axial velocity for various Re_L at $y = 2.0$ mm; $\beta = 1°$.

the turbulence intensity exhibits a maximum value between 2.8 and 3.0 at a distance $y^+ \sim 13$ over a wide range of Reynolds numbers (e.g. Ueda and Hinze, 1975; Kreplin and Eckelmann, 1979). The increase of the turbulence intensity relatively close to the interface ($y^+ > 50$) can be attributed to the influence of the interfacial 3D high-frequency small-amplitude waves on the velocity fluctuations, which may be regarded as *wave induced turbulence* (Karimi and Kawaji, 1999).

Based on all the evidence reported so far, it appears that the solitary waves, emerging on the interface at $Re_{LC} \sim 2100$ for all inclination angles and tube diameters tested (Table 2), may be

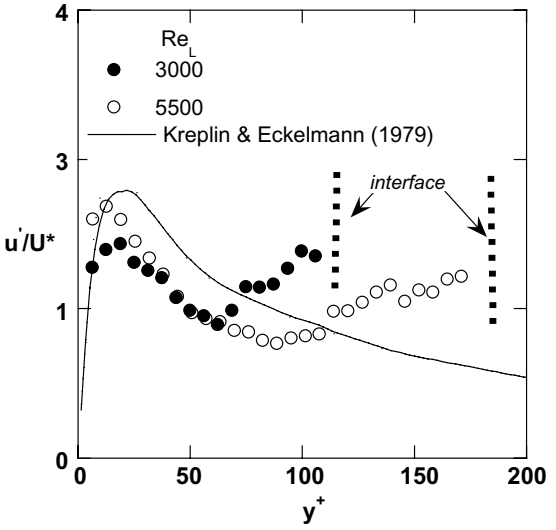

Fig. 11. Turbulence intensity distribution for various flow rates; $\beta = 1°$.

attributed to the transition from laminar-to-turbulent flow inside the liquid layer. The intermittent appearance of the solitary waves bears noteworthy similarities to the events associated with, and concepts employed to describe, the laminar to turbulent transition in single-phase pipe flow; i.e.:

- The "*puffs*" which are defined by Wygnaski and Champagne (1973) "*...as the turbulent regions which are convected downstream ... and represent an incomplete relaminarization process at* $2000 < Re_L < 2700$*...*"
- The "*traveling waves*" which "*...may indeed capture the nature of fluid turbulence... and travel in the streamwise direction*" as reported by Hof et al. (2004).

4. Two-phase co-current gas–liquid downflow

4.1. Liquid layer characteristics

In this section an overview of the liquid layer interfacial structure is presented in co-current gas–liquid downflow, obtained *both* by visual observations and thickness measurements in a 24-mm i.d. pipe and for a range of pipe inclinations ($\beta = 1$–$8°$). The liquid layer thickness was measured for various liquid ($U_{SL} = 1$–20 cm/s) and gas ($U_{SG} = 2$–15 m/s) flow rates and for a range of inclination angles ($\beta = 1$–$8°$). Henceforth the superficial liquid Reynolds number (Re_{SL}) and the superficial gas Reynolds number (Re_{SG}) will be used as a measure of liquid and gas flow rate, respectively. The time series of the layer thickness are statistically analyzed to obtain h_{mean}, h_{rms}, c and f_m (as described in Section 3.2).

A brief account of visual observations is provided here. In the tests, for a given gas flow rate (e.g. $U_{SG} = 3$ m/s) the liquid flow rate is gradually increased. For the smallest liquid rates

employed, small-amplitude waves are observed on the liquid surface (*Region I*). The undisturbed *Region II* observed for the free flowing liquid layer case disappears in two-phase flow. As the liquid flow rate increases (*Region III*), solitary waves (similar to the ones observed in the case of free flowing liquid layer) make their appearance, while small-amplitude waves are present between them. As the liquid flow rate increases further, these large waves become more frequent, retain their original amplitude and merge forming 3D structures (*Region IV*). However, at high gas flow rates (i.e. $U_{SG} > 5$ m/s) and for high liquid flow rates (e.g. $U_{SL} > 10$ cm/s) large-amplitude fast-moving roll waves make their appearance. It is noted that the transition between the regions is *shifted* to lower liquid flow rates as pipe inclination and gas flow rate increase.

In Fig. 12 typical liquid layer traces for $\beta = 1°$ are presented. Fig. 12a corresponds to free flowing water layer, i.e. $U_{SG} = 0.0$ m/s ($Re_L = 2000$, $U_{SL} = 2$ cm/s), with a smooth interface (*Region II*). By increasing the gas flow rate to $U_{SG} = 3.0$ m/s the liquid layer thickness decreases leading to

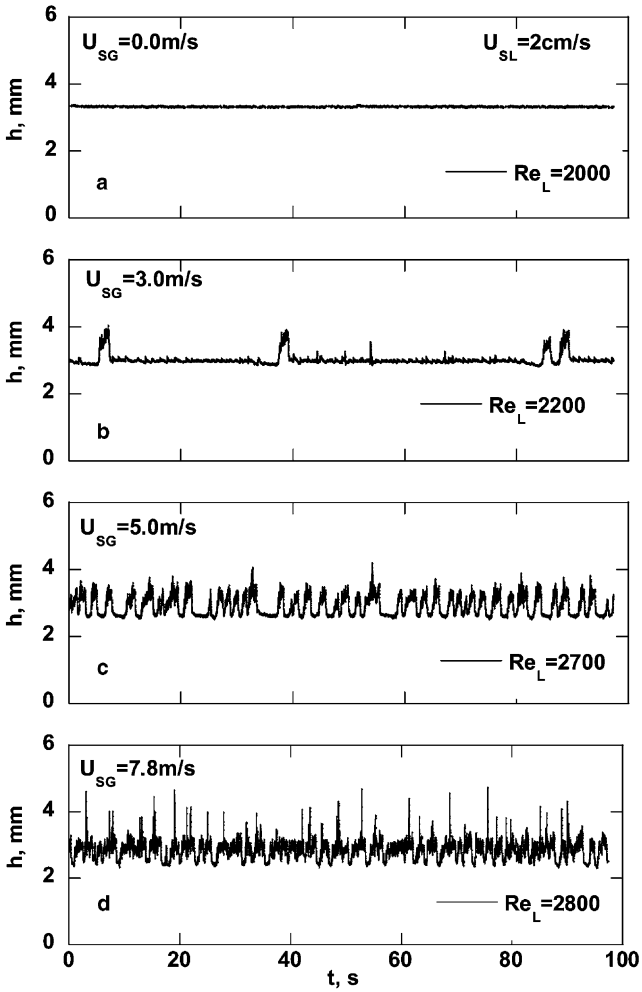

Fig. 12. Typical layer thickness traces for increased gas flow rate; $\beta = 1°$.

Table 3
Effect of pipe inclination on Re_{LC}, for various gas flow rates (two-phase flow)

β (deg)	U_{SG} (m/s)					
	3	5	7	9	11	13
1	2200	2130	2150	2050		
4	2200	2300	2050	2050	2000	2100
8	2300	2300	2100	2000	2000	2000

an increase of the *actual* Reynolds number ($Re_L = 2200$), and the first solitary waves appear while the rest of the interface is covered with small-amplitude waves (Fig. 12b). As the gas flow rate further increases ($U_{SG} = 5.0$ m/s), Re_L becomes even larger ($Re_L = 2700$) and the large-amplitude waves become more frequent (Fig. 12c). Finally, at still higher gas flow rates ($U_{SG} = 7.8$ m/s) the large waves merge forming 3D waves, as shown in Fig. 12d. The above behavior is observed for all pipe inclinations employed.

The solitary waves, which are periodically emerging, are related to the transition from laminar to turbulent flow, as described in Section 3.3, for the free flowing liquid layer case. Both liquid layer thickness measurements and visual observations reveal that the transition from smooth to wavy stratified co-current two-phase flow occurs in the narrow range of Re_L between 2000 and 2300 (Table 3), which is similar to the range that the solitary waves appear in free falling layers. Taitel and Dukler (1976) proposed a model for predicting the transition from smooth to wavy stratified region and suggested that the waves are caused by the gas flow as a result of energy transfer between gas and liquid phase. However, Barnea et al. (1980) observed that waves are present on the liquid interface in inclined geometries even in the absence of gas flow. The findings of the present study suggest that, since the inception of solitary waves is related to the transition from laminar to turbulent flow inside the liquid layer, the gas flow may trigger their emergence in an indirect way by affecting the liquid layer mean thickness and velocity and consequently the corresponding Re_L.

The mean thickness (h_{mean}) of the liquid layer vs. the corresponding Re_{SL} is presented in Fig. 13 for $\beta = 1°$ and 4°. It is evident that h_{mean} decreases as the gas flow rate and the inclination angle increase. The measured h_{mean} values are compared with those calculated using a procedure proposed by Andritsos and Hanratty (1987) and recently revised by Ottens et al. (2001); very good agreement (deviation ±5%) is obtained for all the data sets.

The dependence of h_{rms} on Re_{SL} is presented in Fig. 14, for various gas flow rates and $\beta = 1°$ and 4°. The regions previously identified by both visual observations and liquid layer thickness traces can be distinguished as follows:

- *Region I* corresponds to a liquid interface dominated by small-amplitude 2D waves. The modal frequency and the celerity of these waves increase with the gas flow rate as listed in Table 4.
- *Region III* is characterized by the appearance of solitary waves. The frequency of these waves increases whereas their amplitude is reduced, as the gas flow rate is increased (Table 4). This is evident in Fig. 14a where the maximum h_{rms} value corresponding to *Region III* decreases as the gas flow rate increases. This is attributed to the decrease of the wave amplitude due to the higher gas shear. By comparing Fig. 14a and b it can be seen that as the pipe inclination

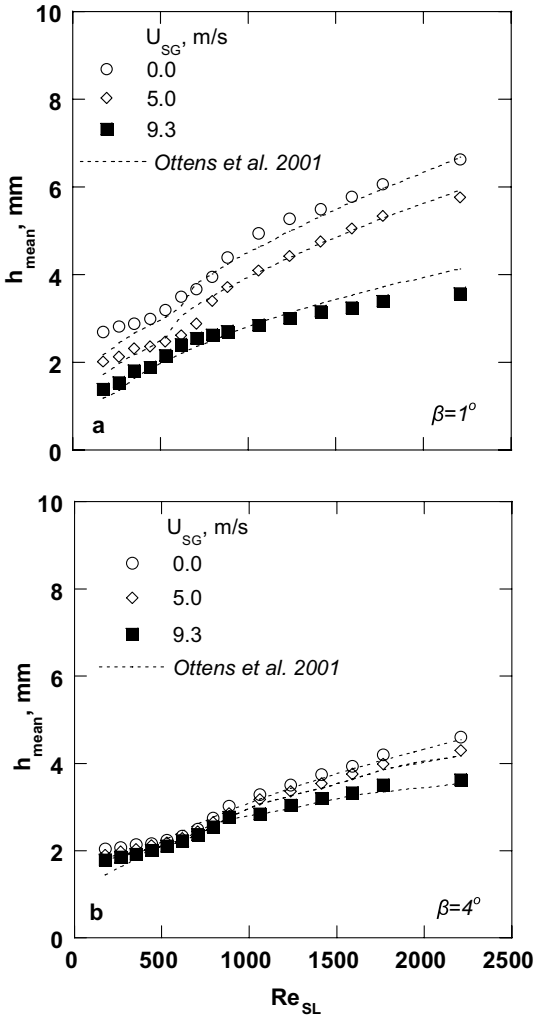

Fig. 13. h_{mean} vs. Re_{SL} for various gas flow rates, comparison with theoretical predictions for various gas flow rates (a) $\beta = 1°$; (b) $\beta = 4°$.

increases, the gas flow influence on the maximum h_{rms} values is less pronounced. Furthermore, from Table 4 it is obvious that as the liquid flow rate increases (for a given gas flow rate) the modal frequency f_m increases.

- *Region IV* corresponds to a liquid layer dominated by 3D waves resulting from the merging of the large waves. As the gas flow further increases, large-amplitude short-wavelength *roll waves* make their appearance. These waves described by various investigators (e.g. Andritsos and Hanratty, 1987; Andritsos, 1992; Brauner and Maron, 1992), are induced by the gas shear and consequently, as the gas flow rate increases, both their amplitude and frequency increase. Moreover, the amplitude of the roll waves is reduced as the pipe inclination increases (Fig. 14).

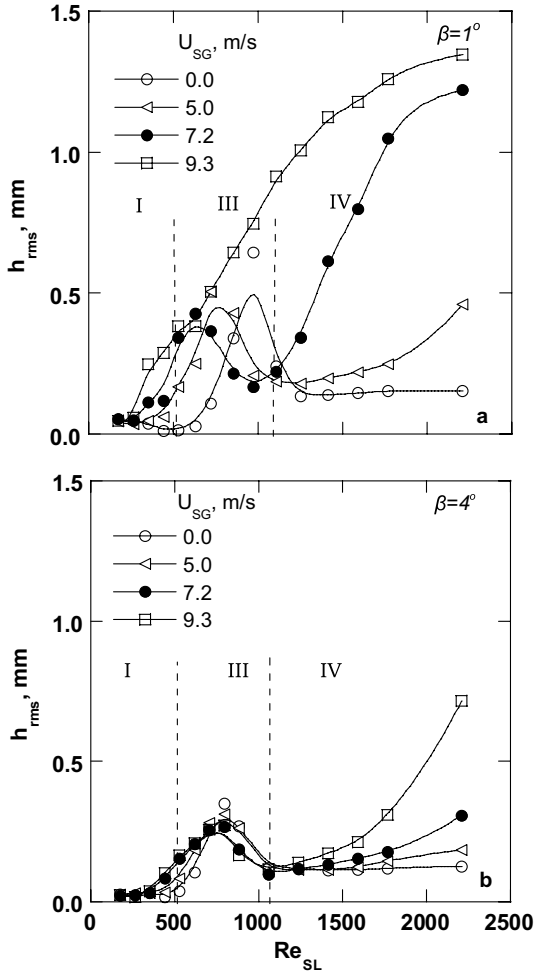

Fig. 14. Effect of gas and liquid flow rate on h_{rms} values: (a) $\beta = 1°$; (b) $\beta = 4°$.

The wave celerity (c) is plotted vs. U_{SG} for a constant liquid flow rate (e.g. $U_{SL} = 7.7$ cm/s) and is compared to the normalized h_{rms}/h_{mean} values (Fig. 15). It is evident that c and h_{rms}/h_{mean} are not significantly affected by the gas flow rate for $U_{SG} < 5.0$ m/s. However, at $U_{SG} > 5.0$ m/s, where the roll waves make their appearance on the gas–liquid interface, c and h_{rms}/h_{mean} sharply increase; this is in agreement with the limited data reported by Andritsos (1992) for gas–liquid stratified horizontal flow.

4.2. Axial velocity measurements in the liquid phase

In order to examine closely the structure of the flow prevailing under the interface in gas–liquid two-phase flow, the local axial velocity inside the liquid layer is measured for various gas and liquid flow rates. Since the interfacial waves induce light reflections on the *LDA* measuring volume,

Table 4
Summary of results (two-phase flow)

Re_{LS}	1°				8°			
	h_{mean} (mm)	h_{rms} (mm)	c (m/s)	f_m (Hz)	h_{mean} (mm)	h_{rms} (mm)	c (m/s)	f_m (Hz)
$U_{SG} = 3$ m/s								
180	2.26	0.11	0.41	0.7				
270	2.59	0.09	0.39	0.6	1.79	0.04	0.41	0.7
350	2.55	0.10	0.42	0.6	1.79	0.04	0.46	0.7
330	2.66	0.11	0.44	0.7	1.72	0.06	0.53	0.8
530	2.81	0.12	0.37	0.7	1.79	0.08	0.56	0.9
620	3.07	0.37	0.47	0.3	1.88	0.14	0.56	0.5
710	3.31	0.48	0.52	0.3	1.99	0.16	0.59	0.4
800	3.58	0.57	0.51	0.3	2.16	0.19	0.64	0.5
880	3.89	0.48	0.52	0.8	2.32	0.17	0.72	1.3
1060	4.32	0.30	0.54	0.9	2.52	0.10	0.75	1.3
1240	4.81	0.22	0.58	0.9	2.79	0.12	0.75	1.4
1410	5.13	0.20	0.60	1.5	2.99	0.13	0.77	2.0
1590	5.45	0.21	0.64	1.8	3.22	0.13	0.80	2.0
1780	5.79	0.23	0.63	1.7	3.42	0.13	0.99	2.1
2210	6.46	0.21	0.62	1.9	3.65	0.13	0.99	2.4
$U_{SG} = 5$ m/s								
180	2.02	0.05	0.58	0.8				
270	2.13	0.04	0.51	0.7				
350	2.31	0.05	0.55	0.7	1.73	0.05	0.58	0.8
330	2.37	0.06	0.62	0.8	1.69	0.09	0.64	0.9
530	2.48	0.17	0.65	0.8	1.78	0.09	0.59	0.9
620	2.62	0.25	0.56	0.4	1.90	0.15	0.56	0.5
710	2.88	0.51	0.56	0.8	1.97	0.17	0.55	0.7
800	3.40	0.43	0.57	0.7	2.12	0.18	0.63	0.8
880	3.72	0.21	0.56	0.8	2.29	0.14	0.62	0.8
1060	4.10	0.19	0.56	1.0	2.50	0.10	0.75	1.1
1240	4.42	0.18	0.64	0.9	2.83	0.13	0.75	1.5
1410	4.76	0.20	0.64	1.5	2.97	0.13	0.80	2.0
1590	5.05	0.22	0.65	1.9	3.21	0.13	0.85	2.1
1780	5.34	0.25	0.64	1.9	3.39	0.13	0.99	2.2
2210	5.77	0.59	0.91	2.1	3.57	0.14	1.20	2.4

it is difficult to make measurements at regions close to the gas–liquid interface. The axial velocity traces at various distances from the pipe wall and for the *Regions I, III, IV* exhibit trends similar to those presented in Fig. 5 for single phase flow, and are not included here for the sake of conciseness.

Fig. 16 presents a comparison of the u' values, (for two typical distances from pipe wall) with the h_{rms} values for a constant gas flow rate ($U_{SG} = 5.0$ m/s) and for various Re_{SL}. It is clear that the h_{rms} distribution exhibits a trend similar to that of u' distribution at a location closer to the interface (i.e. $y = 1.0$ mm); i.e. the peak, corresponding to the solitary wave appearance, occurs at the same Re_{SL} for both h_{rms} and u' distribution. It is noted that the peak in the u' distribution

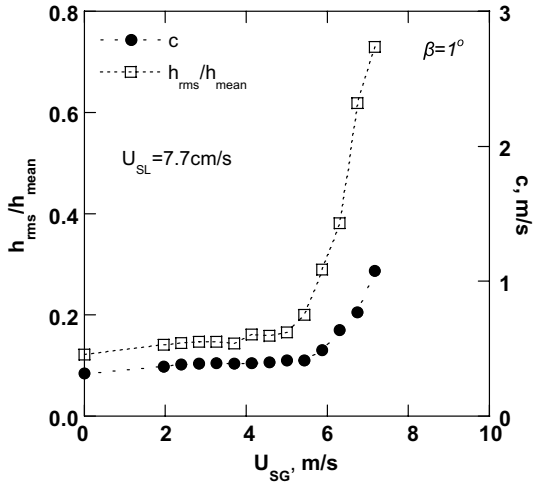

Fig. 15. Comparison of c with $h_{\mathrm{rms}}/h_{\mathrm{mean}}$ for various gas and constant liquid flow rate; $\beta = 1°$.

is less pronounced at a location near the pipe wall (i.e. $y = 0.3$ mm) compared to that at the gas–liquid interface.

The time-average axial velocity ($\overline{U}$) values are plotted in Fig. 17 vs. the normalized distance from the pipe wall (y/h_{mean}), for two gas and liquid flow rates ($U_{\mathrm{SG}} = 3.0$ and 5.0 cm/s and $U_{\mathrm{SL}} = 2$ cm/s and $U_{\mathrm{SL}} = 7$ cm/s). For low liquid rates (e.g. $U_{\mathrm{SL}} = 2$ cm/s), $\overline{U}$ increases significantly, as the gas flow rate increases, only for the region near the gas–liquid interface due to the high gas flow (Fig. 17a). However, in a region near the pipe wall the velocity profile seems to be unaffected by the gas shear. This behavior was also observed by Paras and Karabelas (1991) and Lorencez et al. (1997). The parabolic shape of the velocity profile reveals that the flow is laminar.

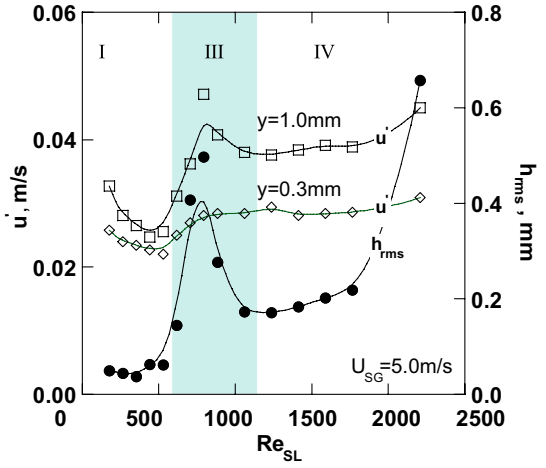

Fig. 16. Comparison of h_{rms} and u' for various Re_{SL}; $\beta = 1°$.

Fig. 17b presents typical axial velocity measurements for relatively high liquid rates (i.e. $U_{SL} = 7$ cm/s). Although the axial velocity values increase in the region where $y/h < 0.3$, they decrease for the region where $y/h > 0.3$. It should be noted that the location of the maximum velocity ($y/h \sim 0.35$ for $U_{SG} = 3$ m/s), is slightly shifted towards the pipe bottom as the gas shear stress increases ($y/h \sim 0.25$ for $U_{SG} = 5$ m/s), probably due to the presence of the waves on the gas–liquid interface. As already mentioned in Section 3.3 the wavy surface fluctuations seem to generate turbulence (as suggested by Karimi and Kawaji, 1999) by creating interfacial turbulent bursts in the thicker liquid layers (Lorencez et al., 1997). There is considerable discussion in the literature (e.g. Fabre et al., 1983; Paras and Karabelas (1992); Banat, 1992; Wongwises and Kalinitchenko, 2002) that these structures create secondary flows inside the liquid flow field, which are characterized by axial velocity components opposed to the main flow. Axial velocity measurements very

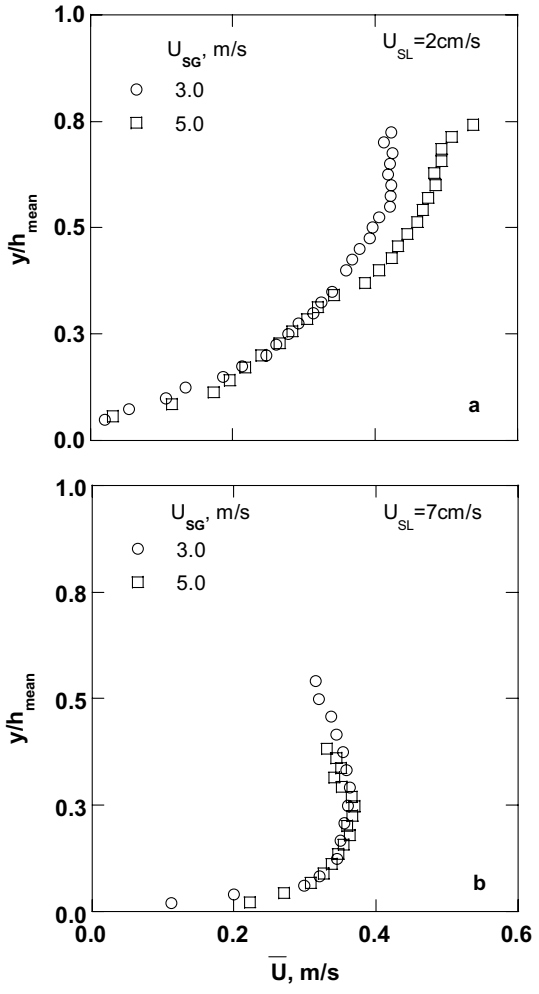

Fig. 17. Time-averaged axial velocity profiles for various gas and liquid flow rates: (a) $U_{SL} = 2$ cm/s; (b) $U_{SL} = 7$ cm/s; $\beta = 1°$.

close to the gas–liquid interface were not made as they are prone to error; indeed, *laser* light reflected at the interface acts as a spurious "reference beam" reaching the photomultiplier and may cause serious errors (Paras and Karabelas, 1992). Nevertheless it is expected that the axial velocity should increase near the gas–liquid interface (e.g. $y/h > 0.7$) since the interfacial shear accelerates the liquid surface layer.

Fig. 18 presents the distribution of the dimensionless velocity (U^+) vs. dimensionless distance (y^+) from the pipe wall. An interesting result for the higher liquid flow rate (i.e. $Re_L = 5800$) is

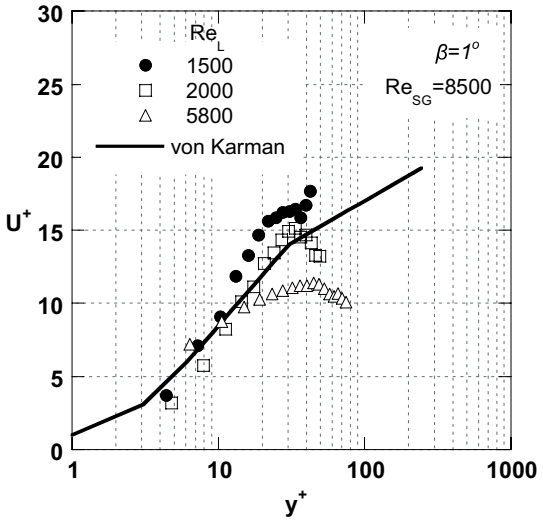

Fig. 18. Comparison of U^+ with von Karman universal velocity distribution for various Re_L (two-phase flow; $\beta = 1°$).

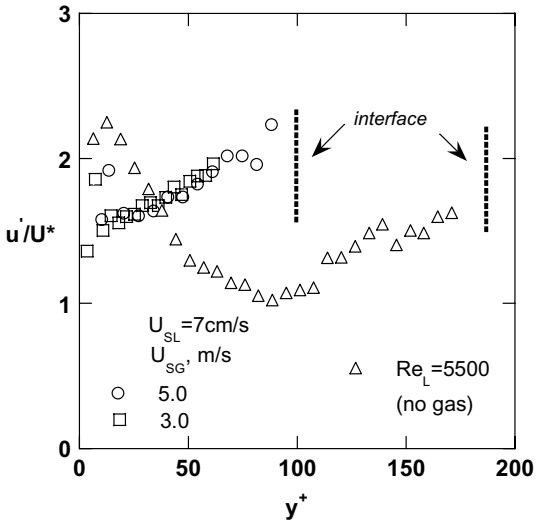

Fig. 19. Turbulence intensity distribution for various gas and liquid flow rates; $\beta = 1°$.

the relatively low U^+ values far from the wall ($y^+ > 20$), as compared with the velocity profile for single-phase flow. Furthermore, it appears that the liquid flow turns from laminar to transitional at lower Re_L ($Re_L \sim 2000$), in the presence of gas flow, than the corresponding Re_L for the free flowing layer ($Re_L \sim 2300$), as seen in Fig. 9. Table 3 suggests that, as the gas flow rate increases the first large wave appears at somewhat lower Re_{LC}, a fact attributed to the growth of disturbances caused by the gas flow.

The turbulence intensity (u'/U^*) is plotted vs. the dimensionless distance (y^+) for the stratified flow experiments (Fig. 19). It is interesting to notice that in the near wall region ($y^+ < 20$) the values of u'/U^* exhibit a maximum $\sim$2 at $y^+ \sim 13$, a behavior similar to the one observed for free flowing layers. In general, u'/U^* tends to increase as the gas/liquid interface is approached, but attains greater values when gas flows co-currently over the liquid. This is attributed to air induced interfacial shear, which significantly affects the flow structure of the liquid phase in the neighborhood of the wavy gas–liquid interface, as compared to free flowing liquid.

5. Concluding remarks

New experimental data on liquid layer thickness and liquid layer flow structure in inclined pipes for various gas–liquid flow conditions have been obtained and are expected to contribute to improved understanding of the mechanisms prevailing in gas–liquid co-current flow in inclined pipes.

For the case of *free flowing liquid*, the visual observations reveal four distinct Re_L regions on the basis of the prevailing wave patterns. A critical Reynolds number, Re_{LC}, is related to the appearance of the first solitary wave which marks the transition from *Region II* to *Region III*. It is observed that these solitary waves first appear in a narrow range of $Re_{LC} \sim 2100$–2300. Axial velocity measurements made with *LDA* in the liquid layer, in conjunction with liquid thickness characteristics, suggest that:

- At small Re_L the liquid flow field, despite the appearance of gravitational small-amplitude waves (*Region I*), maintains typical laminar characteristics before the appearance of solitary waves (*Regions I* and *II*).
- Solitary waves appear to be associated with changes of liquid flow field structure, and more specifically with the transition from laminar to turbulent flow (independent of inclination angle). The intermittent appearance of these waves is directly related to the intermittently occurring turbulent flow within the liquid layer, at Reynolds numbers in the range 2000–3000. Furthermore, it seems that the solitary waves are related to the near-the-wall turbulence produced inside the liquid layer.
- The liquid flow field exhibits typical turbulent characteristics after large wave merging (*Region IV*).

A simplified model based on a modified force balance is proposed for the prediction of the mean layer thickness based on the liquid flow rate, pipe diameter and inclination angle. The proposed model predictions are in good agreement with the experimental data and support the idea that the appearance of solitary waves is related to the transition from laminar to turbulent flow.

For the *co-current gas–liquid downflow* case, it is evident that, as the gas flow rate increases, the mean layer thickness decreases, which is in good agreement with the correlations proposed in the literature. Furthermore, the transition to wavy stratified flow occurs in a narrow Re_L range, somewhat lower than that observed for the appearance of solitary waves in the free flowing layer, which is attributed to disturbance growth by the gas shear. *LDA* measurements made under the wavy gas–liquid interface indicate that the transition to turbulence is again closely associated with the appearance of solitary waves as is the case of free flowing liquid layer. Overall, the new data suggest that solitary waves (even in the presence of air) may emerge as a result of transition to turbulence within the liquid layer. Furthermore, the interfacial gas shear tends to significantly modify the turbulence structure of the liquid phase in the neighborhood of the wavy interface as compared to the free flowing layers.

Acknowledgments

Financial support by the GSRT (*Heracletus Programme*) is gratefully acknowledged. The authors also wish to acknowledge Dr. A.A. Mouza and Mr. A. Lekkas for their significant contribution to this work.

Appendix A. Free flow of a thin liquid layer in inclined tube

The flow geometry is defined in Fig. A1.
The force balance for the liquid phase is

$$-A_L \frac{dP}{dx} - \tau_L S_L - \tau_i S_i + \rho_L A_L g \sin\beta = 0 \tag{A.1}$$

where dP/dx is the average axial pressure gradient, τ_L the wall shear stress, τ_i the interfacial shear stress, S the wetted perimeter, g the gravitational acceleration and ρ_L the liquid density. The following assumptions are made to simplify Eq. (A.1):

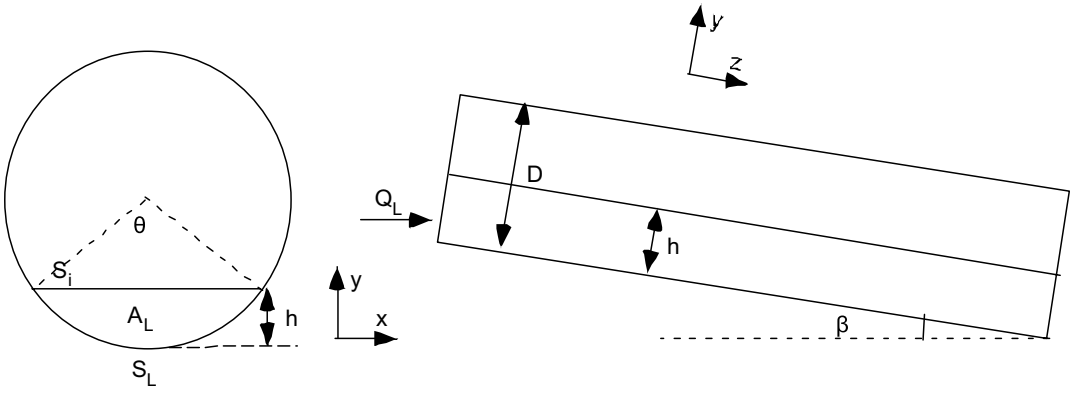

Fig. A1. System coordinates and parameters.

- Flat free surface, with a free flowing layer thickness given by

$$h = \frac{D}{2}(1 - \cos\theta) \tag{A.2}$$

  θ, defined by Fig. A1
- $\tau_i = 0$ and
- $dP/dx = 0$

The shear stress and the liquid friction factor (f_L) are defined in Eqs. (A.3) and (A.4):

$$\tau_L = f_L \frac{\rho_L U_L^2}{2} \tag{A.3}$$

$$f_L = C_L \left(\frac{A_L v_L}{D_L Q_L}\right)^n \tag{A.4}$$

where $D_L = 4A_L/S_L$ is the hydraulic diameter as suggested by Taitel and Dukler (1976). By substituting Eqs. (A.2)–(A.4) in Eq. (A.1), we obtain

$$\frac{S_L^{n+1}}{A_L^3} = \frac{2^{2n+1} g \sin\beta}{C_L Q^{2-n} v_L^n}\theta \tag{A.5}$$

where the constants in the friction factor correlation are $C_L = 0.046$, $n = 0.2$ for *turbulent* flow and $C_L = 16$, $n = 1.0$ for *laminar* flow. Eq. (A.5) is a function of θ and by substituting S_L and A_L (from the pipe geometry):

$$S_L = \theta\frac{D}{2} \quad \text{and} \quad A_L = \frac{D^2}{2}(\theta - \sin\theta) \tag{A.6}$$

Eq. (A.5) becomes

$$\frac{\theta^{n+1}}{(\theta - \sin\theta)^3} = \frac{2^{3n-7} D^{5-n} g \sin\beta}{C_L Q^{2-n} v_L^n} \tag{A.7}$$

and it is solved analytically by applying Taylor-series expansion:

$$\frac{\theta^{n+1}}{(\theta - \sin\theta)^3} = \theta^{n+1}\left(\frac{216}{\theta^9} + \frac{162}{5\theta^7} + \cdots\right) \approx \theta^{n+1}\left(\frac{216 + \frac{162}{5}}{\theta^9}\right) \tag{A.8}$$

Eq. (A.8) is solved for laminar and turbulent flow (using the appropriate coefficients for each case) leading to

$$\theta = 5.155\left(\frac{Q_L v_L}{D^4 g \sin\beta}\right)^{0.142}, \quad \textit{laminar flow} \tag{A.9}$$

$$\theta = 2.480\left(\frac{Q_L^{1.8} v_L^{0.2}}{D^{4.8} g \sin\beta}\right)^{0.128}, \quad \textit{turbulent flow} \tag{A.10}$$

References

Andreussi, P., Persen, L.N., 1987. Stratified gas–liquid flow in downwardly inclined pipe. Int. J. Multiphase Flow 13, 567–575.

Andritsos, N., Hanratty, T.J., 1987. Influence of interfacial waves in stratified gas–liquid flows. AIChE J. 3, 444–454.

Andritsos, N., 1992. Statistical analysis of waves in horizontal stratified gas–liquid flow, Brief communication. Int. J. Multiphase Flow 18, 465–473.

Banat, M., 1992. Experiments of stratified fully developed 2-phase wavy flow. Int. J. Eng. Fluid Mech. 5, 517–532.

Barnea, D., Shoham, O., Taitel, Y., Dukler, A.E., 1980. Flow pattern transition for gas–liquid flow in horizontal and inclined pipes—comparison of experimental data with theory. Int. J. Multiphase Flow 6, 217–225.

Binnie, A.M., 1957. Experiments on the onset of the wave formation on a film of water flowing down a vertical plate. J. Fluid Mech. 2, 551–553.

Brauner, N., Maron, D.M., 1992. Analysis of stratified/non-stratified transitional boundaries in inclined gas–liquid flows. Int. J. Multiphase Flow 18, 541–557.

Fabre, J., Masbernat, L., Suzanne, C., 1983. New results on the structure of stratified flow. In: Proceedings of the 3rd Multiphase Flow and Heat Transfer Conference 1, Miami Beach, FL, pp. 135–154.

Fowler, A.C., Howell, P.D., 2003. Intermittency in the transition to turbulence. SIAM J. Appl. Math. 63, 1184–1207.

Fulford, G.D., 1964. The Flow of Liquids in Thin Films. In: Advances in Chemical Engineering, vol. 5. Academic Press, New York, pp. 151–235.

Giovine, P., Minervini, A., Andreussi, P., 1991. Stability of liquid flow down an inclined tube. Int. J. Multiphase Flow 17, 485–496.

Hof, B., Doorne, C.W.H., Westerweel, J., Nieuwstadt, F.T.M., Faisst, H., Eckhardt, B., Wedin, H., Kerswell, R.R., Waleffe, F., 2004. Experimental observation of nonlinear travelling waves in turbulent pipe flow. Science 305, 1594–1597.

Jones, L.O., Whitaker, S., 1966. Experimental study of falling liquid films. AIChE J. 12, 525–529.

Karimi, G., Kawaji, M., 1998. An experimental study of freely falling films in a vertical tube. Chem. Eng. Sci. 53, 3501–3512.

Karimi, G., Kawaji, M., 1999. Flow characteristics and circulatory motion in wavy falling films with and without counter-current gas flow. Int. J. Multiphase Flow 25, 1305–1319.

Kreplin, H.P., Eckelmann, H., 1979. Behavior of the three fluctuation velocity components in the wall region of a turbulent channel flow. Phys. Fluids 22, 1233–1239.

Lioumbas, J.S., Nydal, O.J., Paras, S.V., 2004. Study of free falling liquid layer in inclined pipes: effect of diameter and inclination angle. In: 3rd International Symposium on Two-Phase Flow Modelling and Experimentation, Pisa, Italy.

Lorencez, C., Nasr-Esfahany, M., Kawaji, M., Ojha, M., 1997. Liquid turbulence structure at a sheared and wavy gas–liquid interface. Int. J. Multiphase Flow 23, 205–226.

Mouza, A.A., Paras, S.V., Karabelas, A.J., 2003. Incipient flooding in inclined tubes of small diameter. Int. J. Multiphase Flow 29, 1395–1412.

Ng, T.S., Lawrence, C.J., Hewitt, G.F., 2001. Gravity-driven laminar flow in a partially filled pipe. Trans. IChem 79, 499–511.

Nino, E., Serio, C., 2000. Laser Doppler velocimetry analysis of transitional pipe flow. Eur. Phys. J. B 14, 191–200.

Ottens, M., Hoefsloot, H.C.J., Hammersma, P.J., 2001. Correlations predicting liquid hold-up and pressure gradient in steady state (nearly) horizontal co-current gas–liquid pipe flow. Trans. IChem 79, 581–592.

Paras, S.V., Karabelas, A.J., 1991. Properties of the liquid layer in horizontal annular flow. Int. J. Multiphase Flow 17, 439–454.

Paras, S.V., Karabelas, A.J., 1992. Measurements of local velocities inside thin liquid films in horizontal two-phase flow. Exp. Fluids 13, 190–198.

Park, C.D., Nosoko, T., 2003. Three-dimensional wave dynamics on a falling film and associated mass transfer. AIChE J. 49, 2715–2727.

Patnaik, V., Blanco, H.P., 1996. Roll waves in falling films: an approximate treatment of the velocity field. Int. J. Heat Fluid Flow, 63–70.

Schlichting, H., Gersten, K., 1999. Boundary Layer Theory, eighth ed. Springer.

Stainthorp, F.P., Allen, J.M., 1965. The development of ripples on the surface of liquid film flowing inside a vertical tube. Trans. Inst. Chem. Eng. 43, T85–T91.

Taitel, Y., Dukler, A.E., 1976. A model for predicting flow regime transitions in horizontal and near horizontal gas–liquid flow. AIChE J. 22, 47–55.

Telles, A.S., Dukler, A.E., 1970. Statistical characteristics of thin vertical wavy liquid films. Ind. Eng. Chem. Fund. 9, 412–421.

Ueda, H., Hinze, J.O., 1975. Fine-structure in the wall region of a boundary layer. J. Fluid Mech. 67, 125–143.

Vlachogiannis, M., Bontozoglou, V., 2002. Observations of solitary wave dynamics of film flows. J. Fluid Mech. 435, 191–215.

Wilkes, J.O., Nedderman, P., 1962. The measurement of velocities in thin films of liquid. Chem. Eng. Sci. 17, 177–187.

Wongwises, S., Kalinitchenko, V., 2002. Mean velocity distributions in a horizontal air–water flow, Brief communication. Int. J. Multiphase Flow 28, 167–174.

Wygnaski, I.J., Champagne, F.H., 1973. On the transition in a pipe. Part 1. The origin of puffs and slugs and the flow in a turbulent slug. J. Fluid Mech. 59, 281–335.